

# Sensitivity Analysis of Multi-Regime Population Balance Model for Control of Multiple Particulate Properties in Granulation

François Févotte and Francis J. Doyle III

**Abstract**—A systematic study of a multi-dimensional model for particle dynamics in a granulation process is detailed. The model accounts for three controlled variables: distributions in particle size, moisture composition, and porosity. Controllability insights are obtained from sensitivity studies involving the properties of the manipulated input: binder addition. Discontinuities in a multi-regime kernel in the model lead to bimodal particle attribute distributions.

## I. INTRODUCTION

Granulation is a widely used chemical engineering process in which small particles agglomerate together into larger granules. In wet granulation processes, the coagulation of particles is improved by the addition of a binder liquid sprayed over an agitated powder in a tumbling drum or pan. The particles are wetted by the binder and nucleate. The resulting binder-coated granules can then collide and stick to each other forming larger granules. These granules can also compact and consolidate as the binder liquid is brought to the surface of the aggregates due to the stirring in the granulator. Particles may also break due to collision with the other particles or the granulator walls during the mixing. Thus, the main phenomena in granulation processes are the granule wetting and nucleation, consolidation and growth, and aggregation and breakage [1].

Granulation processes are widely used in many industries such as pharmaceuticals, agricultural products and fertilizers, among others. Although they have been used and studied over the last 50 years, such processes remain problematical, since they are often operated in a very inefficient manner. Very small yields and large recycle ratios (typically 4:1, recycle:product) are often reported. This mainly comes from the difficulty in designing and controlling granulation circuits allowing maintenance of specified size ranges for the granules. Thus, there are substantial opportunities to improve process design, operation and control.

The most common way of describing the complicated phenomena associated with particle growth and coagulation is to use population balance models, as described in [2]. However, these models typically consist of first-order, partial, integro-differential equations and their solution poses a serious numerical challenge. Another difficulty is caused by the difference in characteristic times for the growth and coagulation of particles, resulting in the stiffness of the Population Balance Equation (PBE). Generic solution

F. Févotte is with ENSTA, 32 boulevard Victor, 75739 PARIS Cedex 15, France; francois.fevotte@ensta.org

F. Doyle is with the Department of Chemical Engineering, UCSB, Santa Barbara, CA 93106, USA; frank.doyle@icb.ucsb.edu

techniques, such as finite difference, finite element and spectral methods have been studied and compared with respect to their efficiency to solve these PBEs by Mantzaris *et al.* ([3], [4] and [5]).

## II. METHODS

### A. Population Balance Equation

The population balance model developed by Immanuel and Doyle to describe the granulation process incorporating nucleation, consolidation and coagulation is employed in this work [6]. The granules are characterized by three internal coordinates: solid volume ( $s$ ), liquid binder volume ( $l$ ), and gas-filled pores volume ( $g$ ). The corresponding population balance equation is given by:

$$\frac{\partial}{\partial t} F(x, t) = -\frac{\partial}{\partial g} \left( F(x, t) \frac{dg}{dt} \right) - \frac{\partial}{\partial l} \left( F(x, t) \frac{dl}{dt} \right) + R_{aggre}^{formation}(x, t) - R_{aggre}^{depletion}(x, t) \quad (1)$$

where  $x = (s, l, g)$  represents the three internal coordinates, and  $F(x, t)$  represents the population density function, defined such that  $F(x, t) dx$  is the moles of granules of solid volume between  $s$  and  $s + ds$ , liquid volume between  $l$  and  $l + dl$ , and gas volume between  $g$  and  $g + dg$ . The partial derivative term with respect to  $t$  in the left hand side accounts for the accumulation of the particles. The partial derivative term with respect to  $g$  accounts for the consolidation phenomenon. Likewise, the partial derivative term with respect to  $l$  accounts for the wetting of the granules due to the spraying of binder liquid.  $R_{aggre}^{formation}(x, t)$  and  $R_{aggre}^{depletion}(x, t)$  respectively account for the gain and loss of particles due to the aggregation phenomenon. The breakage phenomenon has been neglected in this case.

The use of  $(s, l, g)$  coordinates facilitates the formulation of this population balance equation, since the coagulation phenomenon is additive with respect to these coordinates. However, one can use the mapping given by equations (2) and (3) to re-cast these coordinates as the radius ( $r$ ), moisture ( $m$ ), and porosity ( $p$ ) of the granules:

$$\begin{cases} r = \left( \frac{3(s+l+g)}{4\pi} \right)^{\frac{1}{3}} \\ m = \frac{l}{s+l+g} \\ p = \frac{l+g}{s+l+g} \end{cases} \quad (2)$$

$$\begin{cases} s = (1-p) \frac{4\pi r^3}{3} \\ l = m \frac{4\pi r^3}{3} \\ g = (p-m) \frac{4\pi r^3}{3} \end{cases} \quad (3)$$

## B. Model

The consolidation phenomenon accounts for the compaction of the granules due to the stirring in the granulator. Therefore, it results in a decrease of the particle porosity  $p$ , defined as  $p = \frac{l+g}{s+l+g}$ . This evolution is modeled using empirical information, as shown in equation (4), and simplified to equation (5):

$$\frac{dp}{dt} = -c (p - p_{min}) \quad (4)$$

$$\frac{dg}{dt} = -c \frac{s+l+g}{s} [l+g - p_{min}(s+l+g)] \quad (5)$$

where  $c$  is a constant depending upon the mixing parameters in the granulator.

The wetting phenomenon accounts for the effects of the binder fluid spray on the particles. It results in an increase of the liquid volume of the granules. This evolution is modeled through an equal repartition of the binder liquid addition among all the granules, which leads to the wetting rate expression shown in equation (6):

$$\frac{dl}{dt} = \frac{u}{n_{part}} = \frac{u}{\mathcal{N}_A \iiint_{x=x_{nuc}}^{x_{max}} F(x, t) dx} \quad (6)$$

where  $u$  is the binder spray flow,  $n_{part}$  represents the total number of particles in the granulator,  $\mathcal{N}_A$  is Avogadro's number,  $x_{nuc} = (s_{nuc}, 0, 0)$  represents the minimal size of a granule, and  $x_{max} = (s_{max}, l_{max}, g_{max})$  is the maximal size of a granule.

The coagulation phenomenon is taken into account by the formation and depletion rates  $R_{aggre}^{formation}$  and  $R_{aggre}^{depletion}$ :

$$R_{aggre}^{formation}(x, t) = \frac{1}{2} \iiint_{x'=x_{nuc}}^{x-x_{nuc}} c_1 \beta(x', x-x') F(x', t) F(x-x', t) dx' \quad (7)$$

$$R_{aggre}^{depletion}(x, t) = F(x, t) \iiint_{x'=x_{nuc}}^{x_{max}} c_1 \beta(x', x) F(x', t) dx' \quad (8)$$

where  $x_{nuc}$  and  $x_{max}$  are respectively the minimal and maximal size of the granules as previously, and  $\beta(x', x'')$  represents the coagulation kernel, *i.e.* the rate of aggregation of granules of internal coordinates  $x'$  and  $x''$ .

The coagulation kernel is computed using a mechanistic approach, which is described in detail in [7], [6].

## C. Numerical Solution

The numerical method described in [8] and [6] is used in this study. The relative efficiency of this approach over other methods in the literature is described in the original reference. The technique is based on a discretization of the particle size distribution on an arbitrary grid of 'bins' along each one of the internal coordinates  $(s, l, g)$ . In each bin, the particles are assumed to be uniformly distributed — in contrast to the majority of earlier methods, such as the pivot techniques presented in [9] and [10], where the granules are assumed to be concentrated at a single point in each bin. However, a unique representative volume (mid-point) is chosen in each bin to compute the size-dependant properties

(such as the consolidation rates defined in equation (5) and the total volume of the PSD). With these assumptions, a finer grid than usual is required to avoid excessive total volume variation. A sufficient number of finite elements is also required to cover the entire span of the PSD and prevent backward propagation of errors.

At each time step, a first order Euler method is used to update the PSD with respect to the wetting and consolidation phenomena. To overcome the stiffness of the equations, each time step is divided into four equal sub-intervals which are used to update the PSD with respect to the coagulation phenomenon, using a 5-stage predictor-corrector method starting with a first order Euler method and progressively increasing the order of integration.

## III. RESULTS

The previously described mathematical model has been used to study the sensitivity and the controllability of the granulation process. The only manipulated variable defined in this model is the binder addition flow  $u$  appearing in the wetting rate defined by equation (6). However, one also can indirectly influence the system through design parameters, such as those which describe the stirring in the granulator. A variation in the stirring method would for instance modify the modeling constants  $c$  and  $u_0$  respectively used to describe the compaction rate in equation (5) and the coagulation kernel.

### A. Binder Addition (case I)

In this first case, somewhat extreme values of the process parameters are chosen to illustrate the interaction between different phenomena involved in the granulation process. The initial liquid volume of the powder is large whereas the liquid cut-off volume is small ( $l_{ini} \approx \frac{1}{16} l_{cut-off}$ ). This reduces the possible number of successive coagulation events by allowing the granules to be stabilized after only four coagulations. Moreover, the binder addition is constant throughout the entire batch, allowing the granules to reach tremendous moisture levels.

Tracking the final number of particles in the batch yields insight to the number of successive coagulation events: each successful coagulation decreases the number of granules by one. Hence, since the duration of the batch is fixed, a small number of particles at the end of the batch indicates the occurrence of numerous coagulation events, whereas a growth of particles over the cut-off volume prevents them from coagulating and therefore reduces the final number of particles. The evolution of the final total number of particles can be seen on figure 1a. This figure shows an interesting staircase-shaped evolution of the final number of particles. During the continuous steps, the final total number of particles decreases when the binder flow increases. This is easily understandable considering that the coagulation kernel amplitude increases with the solid and liquid volumes.

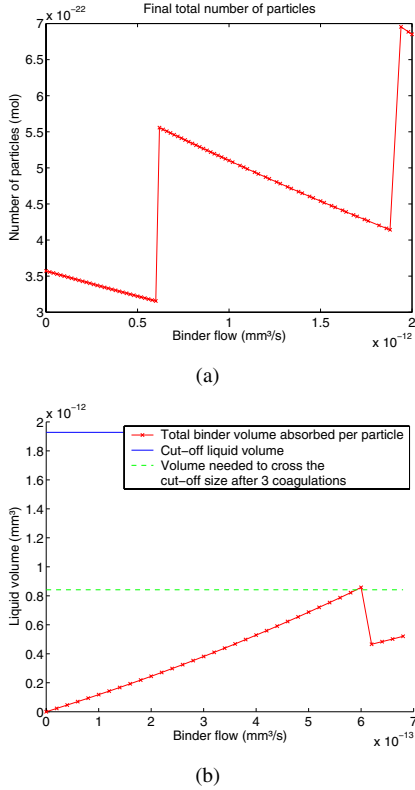


Fig. 1. Simulation of a batch with small cut-off volumes and large initial volumes. Constant binder addition flow throughout the entire batch. Initial number of particles:  $10^{-15}$  mol. (a) Evolution of the final total number of particles in function of the binder addition flow. (b) Total liquid volume absorbed per particle during the batch due to binder liquid spray.

However, more interpretation is needed to explain the discontinuities of the curve. The coagulation phenomenon is intrinsically of a discrete nature: if all the particles have the same initial volume, the volume of the particles resulting from coagulation will always be a whole multiple of the initial volume. One can thus expect the PSD to present local maxima for all the whole multiples of the initial size. In particular, numerous granules will result from three successive coagulation and thus be eight times as big as the initial volume. One can calculate the binder liquid volume missing to these granules to reach the liquid cut-off volume. One can also compute the total volume absorbed per particle during the batch (figure 1b). These two curves cross exactly for the same binder addition flow that caused the discontinuity of the final number of granules in figure 1. Thus, for this value of the binder addition flow, a non-negligible part of the Particle Size Distribution is stabilized at the same time, causing a sudden decrease in the coagulation.

This result leads to the conclusion that two antagonistic phenomena are involved in granulation processes:

- 1) the wetting of the particles improves the coagulation by shifting the granules towards the high liquid volumes, in an area where the coagulation kernel is

higher

- 2) an excessive binder addition leads to the stabilization of the granules.

The extremely low number of successive coagulation events allowed in this case leads to the emphasis of the discrete nature of the stabilization phenomenon, thus allowing one to distinguish between these two phenomena.

### B. Binder Addition (case II)

In the present section, the system response to a rectangular pulse of binder addition is studied. The simulation parameters used are more realistic, with a small initial size of the powder particles and a large cut-off size. The batch length is  $t_{end} = 2000$  s. The liquid binder addition flow profile is a rectangular pulse during  $\Delta t_{pulse} = \frac{t_{end}}{5} = 400$  s.

In a first simulation, the pulse of binder addition occurs at the beginning of the batch, and is given by:

$$u(t) = \begin{cases} u_{pulse} & \text{if } 0 \leq t \leq \Delta t_{pulse} \\ 0 & \text{if } \Delta t_{pulse} < t \leq t_{end} \end{cases} \quad (9)$$

The evolution of the final number of particles is shown in figure 2. As seen previously, the moderate binder addition flows help improving the coagulation phenomenon, whereas excessive binder addition leads to stabilization of the granules and causes the final total number of particles to increase. However, in this case, the effect of the stabilization phenomenon on the final number of granules has been obscured by the large number of coagulations.

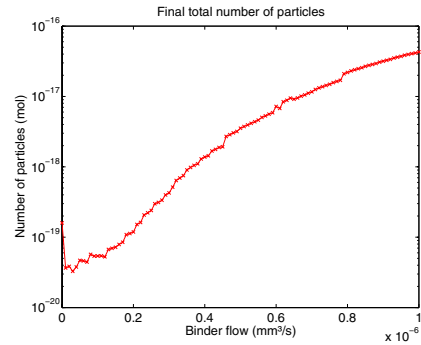


Fig. 2. Final total number of particles in function of the amplitude of a rectangular pulse of binder addition at the beginning of the simulation. (initial number of particles:  $10^{-15}$  mol).

In order to study the response of the system in terms of the particle size distribution, it is useful to reduce the number of dimensions of the PSD. This can be done by integrating the PSD along some of the coordinates:

$$\begin{aligned} F_{s,l}(s, l, t) &= \int_{g=0}^{g_{max}} F(s, l, g, t) dg \\ F_s(s, t) &= \int_{l=0}^{l_{max}} \int_{g=0}^{g_{max}} F(s, l, g, t) dg dl \\ F_l(l, t) &= \int_{s=s_{nuc}}^{s_{max}} \int_{g=0}^{g_{max}} F(s, l, g, t) dg ds \\ F_g(g, t) &= \int_{s=s_{nuc}}^{s_{max}} \int_{l=0}^{l_{max}} F(s, l, g, t) dl ds \end{aligned}$$

where  $F_s$ ,  $F_l$ , and  $F_g$  are the population density functions with respect to the three coordinates  $s$ ,  $l$ , and  $g$ . Thus

$F_s(s, t) ds$  represents the moles of granules of solid volume between  $s$  and  $s + ds$  at instant  $t$ . Likewise,  $F_{s,l}(s, l, t) ds dl$  represents the moles of granules of solid volume between  $s$  and  $s + ds$  and liquid volume between  $l$  and  $l + dl$  at instant  $t$ .

The level curves of the function  $F_{s,l}$  illustrate the shape of the PSD. Figure 3a shows the level curves of  $F_{s,l}$  at final instant  $t_{end} = 2000$  s. without any binder addition. Note that the PSD spread in a diagonal direction from the initial volume of the powder particles at the lower left corner of the figure. This is due to the fact that the coagulation phenomenon is additive with respect to the solid and liquid volumes. One can define a “direction of spreading” of the PSD by considering the difference between two coagulating particles and the resulting granule as explained in figure 4: if two particles  $x_1$  and  $x_2$  coagulate, the resulting particle will be  $x = (s_1 + s_2, l_1 + l_2, g_1 + g_2)$ . The averaged coagulating particle is  $\tilde{x} = (\frac{s_1 + s_2}{2}, \frac{l_1 + l_2}{2}, \frac{g_1 + g_2}{2})$ . Thus, the direction of spreading is  $d_0 = x - \tilde{x} = \frac{1}{2}(s_1 + s_2, l_1 + l_2, g_1 + g_2)$ .

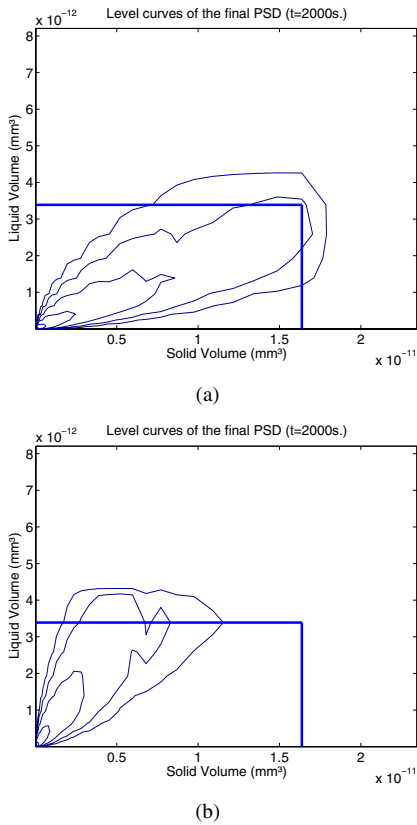


Fig. 3. Level curves of the integrated PSD  $F_{s,l}$  at final instant  $t_{end} = 2000$  s. The thick line represents the cut-off volumes. The binder addition profile is a rectangular pulse during the first 400 s of the batch. (a) No binder addition:  $u_{pulse} = 0$ . (b)  $u_{pulse} = 10^{-8} \text{ mm}^3 \cdot \text{s}^{-1}$

Figure 3b shows the same level curves for a binder addition pulse at the beginning ( $u_{pulse} = 10^{-8} \text{ mm}^3 \cdot \text{s}^{-1}$ ). Note that the binder addition caused the PSD to spread in a different direction, closer from the vertical, liquid volume axis. This is due to the fact that the binder addition occurs at

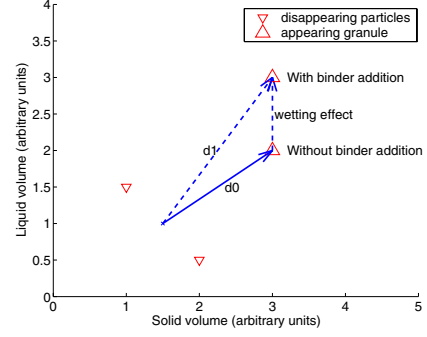


Fig. 4. Definition of the “direction of spreading” of the PSD.

the beginning of the batch, during the coagulation. Thus, if two particles  $x_1$  and  $x_2$  coagulate, the resulting particle will be  $x = (s_1 + s_2, l_1 + l_2 + \frac{u_{pulse}}{n_{part}}, g_1 + g_2)$ , and the direction of spreading is  $d_1 = d_0 + \frac{u_{pulse}}{n_{part}} \delta t (0, 1, 0)$ , where  $\delta t$  represents the characteristic time of coagulation (Figure 4).

The study of the shape of the integrated PSD  $F_s$  and  $F_l$  thus shows a sharpening of the PSD along the solid and gas volume coordinates (Figures 5a and 5c), and a widening of the PSD along the liquid volume coordinate (Figure 5b).

One can also study the system response to a pulse of binder addition occurring in the middle or at the end of the batch. In this latter case, the binder addition profile is given by:

$$u(t) = \begin{cases} 0 & \text{if } 0 \leq t < t_{end} - \Delta t_{pulse} \\ u_{pulse} & \text{if } t_{end} - \Delta t_{pulse} \leq t \leq t_{end} \end{cases} \quad (10)$$

As previously, the final number of particles shows a first decrease followed by an increase as the binder addition flow becomes excessive (Figure 6). The level curves of the integrated PSD  $F_{s,l}$  reveal that in this case, the whole PSD has been shifted towards the high liquid volumes (Figure 7). This can be explained by the fact that the binder addition begins at the end of the batch, at a stage when most of the particles have coagulated several times already. Thus the PSD spreads at first in the direction  $d_0$  until the beginning of the binder addition. After this, the direction of spreading mostly shifts the PSD upwards (*i.e.*, towards higher volumes).

Also note the difference in the orders of magnitude for the binder addition flows:  $10^{-8} \text{ mm}^3 \cdot \text{s}^{-1}$  seems to be a good scale to study the binder addition at the beginning, whereas the binder addition at the end of the batch has to be studied with much smaller flows, such as  $10^{-10} \text{ mm}^3 \cdot \text{s}^{-1}$ . This is due to the fact that the wetting rate defined in equation (6) is inversely proportional to the number of particles, which is smaller at the end of the batch.

### C. Coagulation Kernel Amplitude

Although the binder addition flow is the only manipulated variable explicitly incorporated in the model, one can study the sensitivity of the system with respect to various model

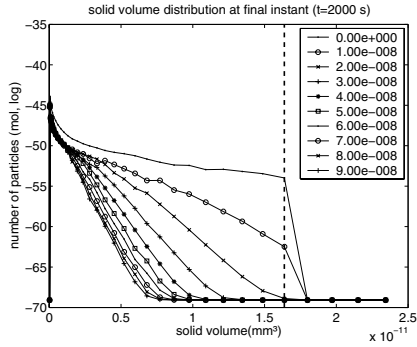
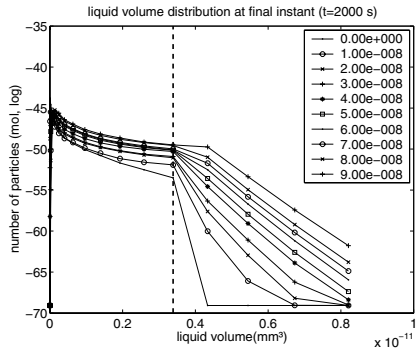
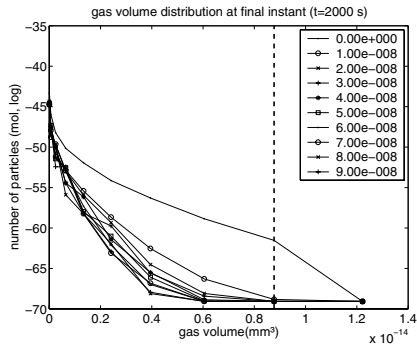
(a)  $F_s$ (b)  $F_l$ (c)  $F_g$ 

Fig. 5. Integrated PSDs ( $F_s$ ,  $F_l$ , and  $F_g$ ) for different amplitudes of the binder addition pulse at the beginning of the batch. The dashed line represents the cut-off volume.

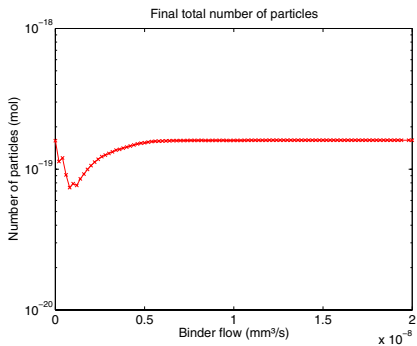
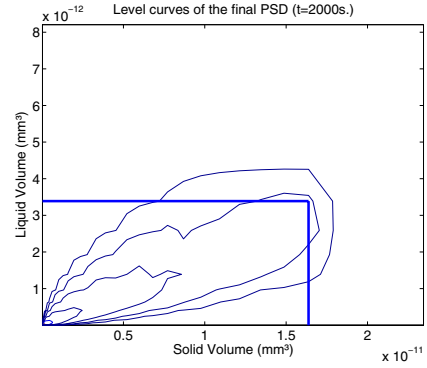
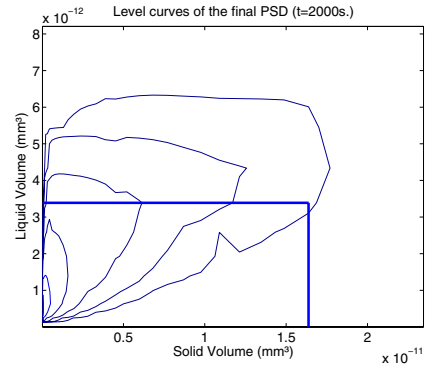


Fig. 6. Final total number of particles in function of the amplitude of a rectangular pulse of binder addition at the beginning of the simulation. (initial number of particles:  $10^{-15}$  mol).



(a)



(b)

Fig. 7. Level curves of the integrated PSD  $F_{s,l}$  at final instant  $t_{end} = 2000$  s. The thick line represents the cut-off volumes. The binder addition profile is a rectangular pulse during the last 400 s of the batch. (a) No binder addition:  $u_{pulse} = 0$ . (b)  $u_{pulse} = 2 \times 10^{-10} \text{ mm}^3 \cdot \text{s}^{-1}$

parameters, since they can be indirectly affected by design parameters, such as the type of stirring device, the stirring rate, or the number and location of the sprinklers.

In the present section, the sensitivity of the system is studied with respect to the amplitude of the coagulation kernel, determined by the model parameter  $c_1$ . The coagulation kernel amplitude  $c_1$  may be influenced by the stirring parameters.

The level curves of the final PSD shown in figure 8 reveal the progressive appearance of multi-modal character in the particle size distribution. As noted previously, the first mode corresponds to the initial size of the particles. The other modes correspond to particles that are just above the liquid cut-off volume. This phenomenon can also be seen on the single-coordinate distributions: with small coagulation kernel amplitude, the particle distributions are very sharp, since no coagulation creates big particles. As the coagulation kernel amplitude increases, the distributions widen until they reach the cut-off volumes, for  $c_1 \simeq 4 \times 10^{11} \text{ mm}^3 \cdot \text{mol}^{-1} \cdot \text{s}^{-1}$ . After this point, the distribution cease widening, and begin changing shape. The solid volume distribution shows the progressive appearance of several modes below the cut-off volume. On the other hand, the liquid volume distribution reveals the appearance

of only one other mode, just above the cut-off volume. The gas volume distribution remains unimodal, as before.

#### IV. SUMMARY

A systematic analysis of the sensitivity of a multi-dimensional population balance model to parameters reflecting manipulated inputs (binder addition, stirring characteristics) reveals the controllability of the evolving distributions. It has been shown that the binder liquid flow directly influences the orientation of the final PSD; while the stirring parameters indirectly influence the final PSD and lead to the appearance of a multimodal distribution.

The results point to the limitations of reachable distributions in size, moisture composition, and porosity using the manipulated inputs. Future studies will address the design of controllers to regulate the particle distributions in the regions described in this study.

#### V. ACKNOWLEDGMENTS

FJD acknowledge financial support from the International Fine Particles Research Institute (IFPRI), and helpful discussions with Jim Litster and Paul Mort.

#### REFERENCES

- [1] S. M. Iveson, J. D. Litster, K. Hapgood, and B. J. Ennis, "Nucleation, growth and breakage phenomena in agitated wet granulation processes: A review," *Powd. Tech.*, vol. 117, pp. 3–39, 2000.
- [2] D. Ramkrishna, *Population Balances*. San Diego: Academic Press, 2000.
- [3] N. V. Mantzaris, P. Daoutidis, and F. Sreic, "Numerical solution of multivariable cell population balance models: I. finite differences methods," *Comput. Chem. Eng.*, vol. 25, pp. 1411–1440, 2001.
- [4] —, "Numerical solution of multivariable cell population balance models: II. spectral methods," *Comput. Chem. Eng.*, vol. 25, pp. 1441–1462, 2001.
- [5] —, "Numerical solution of multivariable cell population balance models: III. finite element methods," *Comput. Chem. Eng.*, vol. 25, pp. 1463–1481, 2001.
- [6] C. D. Immanuel and F. J. Doyle III, "Solution technique for a multidimensional population balance model describing granulation processes," *Powd. Tech.*, Accepted.
- [7] L. X. Liu, J. D. Litster, S. M. Iveson, and B. J. Ennis, "Coalescence of deformable granules in wet granulation processes," *AIChE J.*, vol. 46, no. 3, pp. 529–539, 2000.
- [8] C. D. Immanuel and F. J. Doyle III, "Computationally efficient solution of population balance models incorporating nucleation, growth and coagulation," *Chem. Eng. Sci.*, vol. 58, pp. 3681–3698, 2003.
- [9] S. Kumar and D. Ramkrishna, "On the Solution of Population Balance Equations by Discretization-I. A Fixed Pivot Technique," *Chem. Eng. Sci.*, vol. 51, no. 8, pp. 1311–1332, 1996.
- [10] —, "On the Solution of Population Balance Equations by Discretization - II. A Moving Pivot Technique," *Chem. Eng. Sci.*, vol. 51, no. 8, pp. 1333–1342, 1996.

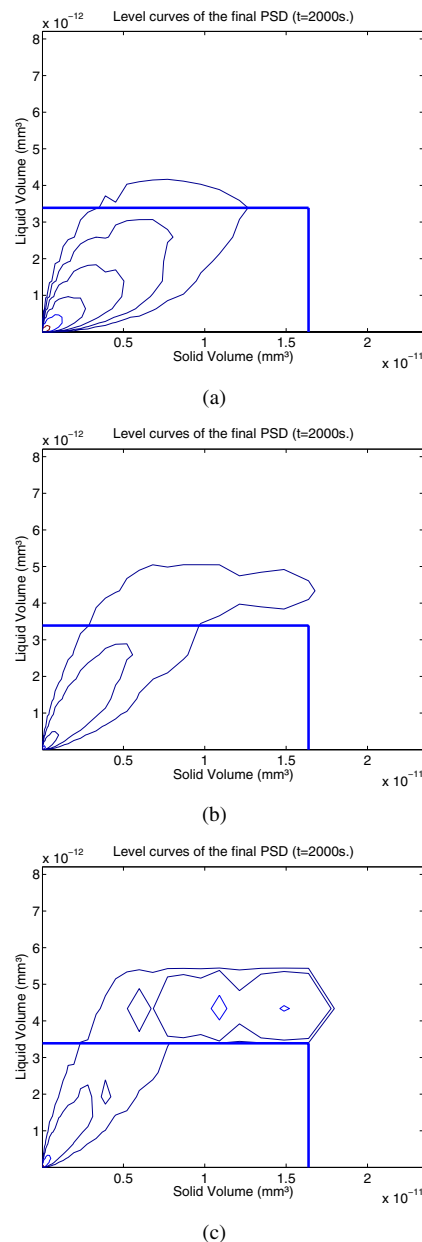


Fig. 8. Level curves of the integrated PSD  $F_{s,l}$  at final instant  $t_{end} = 2000$  s. The thick line represents the cut-off volumes. The binder addition profile is a rectangular pulse during the first 400 s of the batch;  $u_{pulse} = 10^{-8} \text{ mm}^3 \cdot \text{s}^{-1}$ . (a)  $c_1 = 3 \times 10^{11} \text{ mm}^3 \cdot \text{mol}^{-1} \cdot \text{s}^{-1}$ . (b)  $c_1 = 7.5 \times 10^{11} \text{ mm}^3 \cdot \text{mol}^{-1} \cdot \text{s}^{-1}$ . (c)  $c_1 = 9 \times 10^{11} \text{ mm}^3 \cdot \text{mol}^{-1} \cdot \text{s}^{-1}$